

APSeg: Auto-Prompt Model with Acquired and Injected Knowledge for Nuclear Instance Segmentation and Classification

Liyang Xu¹, Hongliang He¹(✉), Wei Han¹, Hanbin Huang¹, Siwei Feng¹, and Guohong Fu¹

School of Computer Science and Technology, Soochow University
hlhe2023@suda.edu.cn

Abstract. Nuclear instance segmentation and classification provide critical quantitative foundations for digital pathology diagnosis. With the advent of the foundational Segment Anything Model (SAM), the accuracy and efficiency of nuclear segmentation have improved significantly. However, SAM imposes a strong reliance on precise prompts, and its class-agnostic design renders its classification results entirely dependent on the provided prompts. Therefore, we focus on generating prompts with more accurate localization and classification and propose **APSeg**, Auto-Prompt model with acquired and injected knowledge for nuclear instance **Segmentation** and classification. APSeg incorporates two knowledge-aware modules: (1) Distribution-Guided Proposal Offset Module (**DG-POM**), which learns distribution knowledge through density map guided, and (2) Category Knowledge Semantic Injection Module (**CK-SIM**), which injects morphological knowledge derived from category descriptions. We conducted extensive experiments on the PanNuke and CoNSEP datasets, demonstrating the effectiveness of our approach. The code will be released upon acceptance.

Keywords: Nuclear detection · Multi-modality model · Nuclear instance segmentation · Segment Anything Model

1 Introduction

Accurate and automated nuclear segmentation and classification is fundamental for clinical pathological image analysis and diagnosis, providing important quantitative results for tasks such as survival rate prediction and cancer staging and grading [7,1]. Segmentation of densely packed, small-volume nuclei and the recognition of subtle category differences is a non-trivial task. Traditional deep learning methods often rely on encoder-decoder structures like U-Net [19], which design different task-aware branches based on the results, such as auxiliary vertical and horizontal distance maps [6], distance maps [9], and topological information [10], to achieve bottom-up instance segmentation and classification with multiple map-assisted methods. However, these methods rely on carefully crafted post-processing, requiring detailed tuning of hyperparameters [26].

Recently, owing to the generalization capabilities of the large vision model SAM [13], fine-tuning based on pre-trained models has greatly reduced the dependency on large datasets. Many SAM-based medical image segmentation models have achieved state-of-the-art (SOTA) performance in areas such as polyps [14,25], tumors [17,20,25], lesions [8,24,15], organs [2], and surgical instruments [27]. In the field of pathological images, CellViT [11] uses pre-trained encoded features as additional knowledge injection, still applying the traditional U-Net architecture; SAC [16] implements an automatic prompt semantic segmentation framework, but still depends on expert prompts and does not achieve instance segmentation; SAMAug [28] leverages SAM’s zero-shot capability for image augmentation, significantly improving the instance segmentation performance of expert models; PromptNucSeg [21] leverages the interactive segmentation capabilities of SAM, achieves a prompt-driven instance segmentation model. However, SAM-based instance segmentation introduces a severe dependency on precise prompts.

To address this issue, we focus on designing a nuclear auto-prompter that better adapts to SAM by learning representations of the pathological image microenvironment. Thus, we propose APSeg: an auto-prompt model with acquired and injected knowledge for nuclear instance segmentation and classification. In APSeg, we introduce two knowledge-aware modules: Distribution-Guided Proposal Offset Module (DG-POM) leverages the nuclear counting task to help the model acquire knowledge of nuclear distribution in pathological images, generating distribution-guided deformed proposals to enhance the sampling features for regression and classification tasks; and Category Knowledge Semantic Injection Module (CK-SIM) focuses on injecting detailed nuclear morphological knowledge using the pre-trained CLIP model [18], thereby improving the classification accuracy of prompts.

In summary, our contributions are as follows: (1) We build an auto-prompt model named APSeg, a novel nuclear auto-prompter designed for nuclear instance segmentation and classification. (2) We propose two modules, DG-POM and CK-SIM, separately augment nuclear detection and classification precision through acquired and injected knowledge. (3) We conduct extensive experiments on the PanNuke and CoNSEP datasets, achieving state-of-the-art performance.

2 Method

Problem Definition. Given an input image $I \in \mathbb{R}^{H \times W \times 3}$ and the corresponding prompts $P = \{p_i\}_{i=1}^N$ where $p_i = ((x_i, y_i), c_i)$, and $c_i \in C$, labeling the position (x_i, y_i) and category c_i of the i -th instance. Nuclear instance segmentation is required to follow the prompts to identify each individual instance i and produce the result map $M_i \in \mathbb{R}^{H \times W}$, where each pixel $M_i(x, y) \in \{0, 1, 2, \dots, i, \dots, N\}$ represents the instance identifier to which the pixel belongs, with 0 denoting the background and i representing a specific instance ID. Our core focus is on how to obtain prompts P that are more accurate in both localization and classification to guide nuclear segmentation.

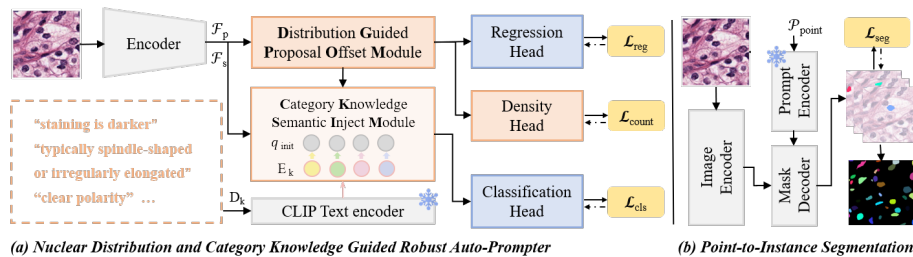


Fig. 1. Overview of APSeg. (a) APSeg consists of two knowledge-aware modules DG-POM and CK-SIM, with a (b) point-to-instance SAM for instance segmentation followed the prompt generated by APSeg.

Framework Overview. The novel auto-prompt framework APSeg is as figured in Fig.1(a), the Segment Anything Model used for nuclear segmentation followed its original design as figured in Fig.1(b). We adopt the method from [21] to design a fine-tuned SAM for point-to-instance task modeling, where all point prompts during testing are generated by APSeg. APSeg introduces an acquired and injected knowledge guided approach through two functional modules DG-POM and CK-SIM.

2.1 Distribution Guided Proposal Offset Module

Different nuclei types across tissues exhibit diverse distribution patterns and densities. Under such complex distributions, fixed proposals make the regression task challenging. DG-POM is designed to overcome this challenge.

As illustrated in Fig.2(a), inspired by studies in counting tasks [22,12], density maps effectively capture instance distribution. Therefore, we introduce an additional density map based nuclear counting task in APSeg. The original proposal design is modified as follows:

$$F_p = \phi_{backbone}(I) \quad (1)$$

$$F'_s = \phi_{relu}(\phi_{conv}(\phi_{relu}(\phi_{conv}(F_s)))) \quad (2)$$

$$(\Delta X_p, \Delta Y_p) = \phi_{deform_layer}(sample(F'_s, P_{proposal})) \quad (3)$$

$$P_{deformed_proposal} = P_{proposal} + (\Delta X_p, \Delta Y_p) \quad (4)$$

Shallow feature F_s which extracted from feature pyramid F_p contains more positional information. It is processed by a distribution decoder, composed of stacked convolutional and activation layers, to obtain an updated feature map F'_s . This updated F'_s is used for sampling the initial proposals $P_{proposal}$ and then passed through a separate deform layer $\phi_{deform_layer}(\cdot)$ to compute the proposal offsets $(\Delta X_p, \Delta Y_p)$.

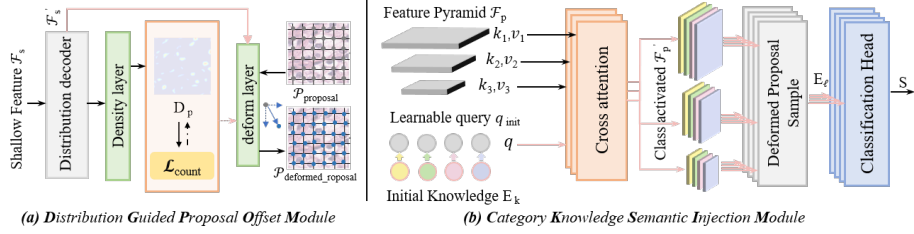


Fig. 2. The detailed architectures of (a) Distribution Guided Proposal Offset module (DG-POM) and (b) Category Knowledge Semantic Injection Module (CK-SIM). The parts of knowledge acquisition and injection are highlighted with pink lines.

The deformed proposals capture the initial nuclear distribution bias, alleviating the burden of regressing real nuclei locations.

$$E_p = \text{sample}(F_p, P_{deformed_proposal}) \quad (5)$$

$$(\Delta X, \Delta Y) = \phi_{reg_head}(E_p) \quad (6)$$

$$P_{point} = P_{deformed_proposal} + (\Delta X, \Delta Y) \quad (7)$$

The predicted points P_{point} matched to ground truth points P_{GT} are supervised, with the matching performed using the Hungarian algorithm.

To enable this process to acquire distribution characteristics, we additionally introduce a density layer $\phi_{density_layer}(\cdot)$ for generating a density map $D_p \in \mathbb{R}^{1 \times 1 \times \frac{H}{2^2} \times \frac{W}{2^2}}$ nuclear instance counting and incorporate a quantity-based loss for supervision:

$$D_p = \phi_{density_layer}(F'_s) \quad (8)$$

$$\mathcal{L}_{count} = MAE(\sum D_p, N) \quad (9)$$

The supervision from the density map regression task and nuclear counting enables the deform layer to effectively learn instance distribution knowledge.

2.2 Category Knowledge Semantic Injection Module

Pathology images contain complex semantic microenvironment information, where nuclei of different categories exhibit subtle morphological differences that are difficult to distinguish, leading to inter-class homogeneity. Inspired by the multimodal pre-trained model CLIP [18] aligns visual and textual semantics, we leverage text to explicitly inject general feature semantic knowledge, aiding in distinguishing inter-class differences and improving nucleus classification.

The pre-trained model CLIP, with general visual-text semantic capabilities, excels at representing basic semantics. Instead of using specialized terminology for nucleus categories, we choose more intuitive morphological descriptions to construct morphological and microenvironmental knowledge for different categories. This knowledge is represented as $E_k = \phi_{text_encoder}(D_k) \in \mathbb{R}^{C \times C_k}$, where

D_k is the description knowledge of C categories, and C_k is the dimensionality of the knowledge text features.

As illustrated in Fig.2(b), we design a method that utilizes a learnable class-aware query $q \in \mathbb{R}^{C \times C_k}$ to activate the feature pyramid F_p and apply E_k as prior knowledge to initialize q . This enables a class-aware query-based comprehensive classification evaluation, ultimately optimizing classification performance. The process is as follows:

$$q' = w_q q, k^l = w_k F_p^l, v^l = w_v F_p^l, l \in \{1, 2, 3\} \quad (10)$$

$$A^l = \text{Softmax}\left(\frac{q'(k^l)^T}{\sqrt{d}}\right) \quad (11)$$

$$(F_p^l)' = A^l v^l \quad (12)$$

where k and v come from the multi layer of the feature pyramid F_p .

After obtaining the class-activated $F_p' \in \mathbb{R}^{C \times C_l \times \frac{H}{2^i} \times \frac{W}{2^i}}$, $i \in \{2, 3, 4\}$ using the class-aware query, the classification is determined separately for the multi-scale feature maps of C classes, and the results are aggregated:

$$E_l^i = \text{Sample}(F_l^i, P_{\text{deformed_proposal}}^i), i \in \{1, 2, \dots, C\} \quad (13)$$

$$S = \phi_{\text{cls_head}}(\phi_{\text{conv}}(\text{Concat}(E_l^i))) \quad (14)$$

where classification result $S \in \mathbb{R}^{N \times (C+1)}$ is supervised using the cross-entropy loss, where w_c is the weight of each categories and c_n is the truth category:

$$\mathcal{L}_{\text{cls}} = - \sum_{n=1}^N w_c \log\left(\frac{e^{S_n, c_n}}{\sum_{c=1}^C e^{S_n, c}}\right) \quad (15)$$

Multi-class aggregation classification, achieved through a category-aware query-activated feature pyramid, ensures the injection of category knowledge.

2.3 Training Loss

The training loss function of APSeg is obtained by weighting the losses of nuclear classification, points regression and instance counting tasks:

$$\mathcal{L} = w_{\text{cls}} \mathcal{L}_{\text{cls}} + w_{\text{reg}} \mathcal{L}_{\text{reg}} + w_{\text{count}} \mathcal{L}_{\text{count}} \quad (16)$$

The regression task is supervised using the L1 loss, where p_n is the location of the n -th nuclei and \hat{p}_n is its ground truth position:

$$\mathcal{L}_{\text{reg}} = \sum_{n=1}^N \|p_n - \hat{p}_n\|_1 \quad (17)$$

Table 1. Performance comparison on the PanNuke dataset, both binary PQ (bPQ) and multi-class PQ (mPQ) are computed. The best and second-best scores are highlighted in **bold** and underlined. The results of PNS(PromptNucSeg) are provided by us.

	HoVer-Net		PointNu-Net		CellViT-H		PNS-H		APSeg	
	bPQ	mPQ	bPQ	mPQ	bPQ	mPQ	bPQ	mPQ	bPQ	mPQ
Tissue										
Adrenal	69.62	48.12	71.34	<u>51.15</u>	70.86	51.34	<u>71.53</u>	50.06	72.10	50.57
Bile Duct	66.96	47.14	68.14	48.68	67.84	48.87	<u>68.98</u>	<u>49.21</u>	69.52	49.82
Bladder	70.31	57.92	<u>72.26</u>	60.65	70.68	58.44	72.38	<u>59.80</u>	71.78	58.94
Breast	64.70	49.02	67.09	51.47	67.48	51.80	68.30	<u>52.07</u>	<u>68.11</u>	52.60
Cervix	66.52	44.38	68.99	<u>50.14</u>	68.72	49.84	<u>69.39</u>	50.12	69.51	50.88
Colon	55.75	40.95	59.45	45.09	59.21	44.85	<u>60.55</u>	<u>45.38</u>	60.75	46.21
Esophagus	64.27	50.85	67.66	55.04	66.82	54.54	<u>68.17</u>	<u>55.37</u>	68.54	55.63
Head & Neck	63.31	45.30	65.46	48.38	65.44	49.13	<u>66.03</u>	<u>50.07</u>	67.02	50.25
Kidney	68.36	44.24	69.12	50.66	70.92	53.66	71.19	<u>54.18</u>	<u>70.94</u>	56.38
Liver	72.48	49.74	73.14	51.74	73.32	52.24	<u>73.45</u>	<u>52.33</u>	73.64	53.11
Lung	63.02	40.04	63.52	40.48	64.26	<u>43.14</u>	<u>65.49</u>	43.01	65.58	43.61
Ovarian	63.09	48.63	68.63	54.84	67.22	53.90	68.23	53.63	<u>68.31</u>	<u>54.21</u>
Pancreatic	64.91	46.00	67.91	48.04	66.58	47.19	68.79	<u>49.34</u>	<u>68.25</u>	49.61
Prostate	66.15	51.01	68.54	51.27	68.21	53.21	69.68	54.73	<u>69.34</u>	<u>53.77</u>
Skin	62.34	34.29	64.94	40.11	65.65	43.39	<u>66.71</u>	<u>41.52</u>	66.75	41.38
Stomach	68.86	47.26	70.10	45.17	70.22	<u>47.05</u>	71.38	46.32	<u>71.23</u>	45.79
Testis	68.90	47.54	70.58	53.34	69.55	51.27	70.99	51.73	<u>70.51</u>	<u>53.08</u>
Thyroid	69.83	43.15	70.76	45.08	<u>71.51</u>	<u>45.19</u>	71.28	44.50	72.31	45.96
Uterus	63.93	43.93	66.34	<u>48.46</u>	66.25	47.37	<u>67.15</u>	46.89	67.20	48.72
Average	65.96	46.29	68.08	49.57	67.93	49.80	<u>68.93</u>	<u>50.01</u>	69.02	50.55
Std	0.36	0.76	0.50	0.82	3.18	4.13	0.10	0.25	0.09	0.23

3 Experiments

3.1 Experimental Setup

Dataset. PanNuke is the largest publicly available dataset for nuclei segmentation and classification [5,4], sourced from The Cancer Genome Atlas (TCGA) and spanning 19 tissue types. It contains 256×256 patches extracted from over 20,000 Whole Slide Images, divided into three folds for training, validation, and testing. Following [5], we replicate the results using the same methodology. Annotations are semi-automatically generated and quality-checked by clinical pathologists to ensure statistical alignment with real-world clinical scenarios and minimal selection bias. CoNSeP [6] consists of 41 images with diverse cell types, categorized into four classes: miscellaneous, inflammatory, epithelial, and spindle-shaped. Following prior studies, it is split into 27 training and 14 testing images.

Implementation Details. Our model is implemented based on the PyTorch framework, and all experiments are performed on a single V100 32GB GPU. For both datasets, we train the APSeG for 300 epochs, with a learning rate set to $1e-4$ with a weight decay of $1e-4$ and the AdamW optimizer used. We set the class

Table 2. Average PQ across three folds for each nuclear category on the PanNuke.

Method	Neoplastic	Epithelial	Inflammatory	Connective	Dead	Average
Mask-RCNN	0.472	0.403	0.290	0.300	0.069	0.307
DIST	0.439	0.290	0.343	0.275	0.000	0.269
StarDist	0.547	0.532	0.424	0.380	0.123	0.401
Micro-Net	0.504	0.442	0.333	0.334	0.051	0.333
HoVer-Net	0.551	0.491	0.417	0.388	0.139	0.397
CPP-Net	0.571	0.565	0.405	0.395	0.131	0.413
PointNu-Net	0.578	0.577	0.433	0.409	0.154	0.430
CellViT-H	0.581	0.583	0.417	<u>0.423</u>	0.149	0.431
PromptNucSeg-H	0.594	<u>0.578</u>	0.410	<u>0.422</u>	0.174	<u>0.436</u>
APSeg	<u>0.592</u>	0.583	<u>0.431</u>	0.425	<u>0.161</u>	0.438

Table 3. Performance comparison on the CoNSEP dataset. The best and second-best scores are highlighted in **bold** and underlined.

Method	Dice	AJI	DQ	SQ	PQ	F_{Det}	F_m	F_i	F_e	F_s
Micro-Net	79.4	52.7	60.0	74.5	44.9	74.3	11.7	59.2	61.5	53.2
Mask-RCNN	-	-	61.9	74.0	46.0	69.2	9.8	59.0	59.5	52.0
DIST	80.4	50.2	54.4	72.8	39.8	71.2	0.0	53.4	61.7	50.5
HoVer-Net	84.5	55.2	68.5	<u>77.5</u>	53.2	73.7	28.6	60.6	62.8	53.5
PointNu-Net	-	-	71.4	76.2	55.5	75.2	46.2	64.7	66.1	55.9
PromptNucSeg	81.0	<u>54.2</u>	68.5	77.7	53.3	75.8	47.7	76.0	68.1	62.9
APSeg	<u>82.3</u>	55.8	<u>70.6</u>	<u>77.5</u>	<u>54.9</u>	76.8	48.0	<u>75.4</u>	69.4	65.4

weights as $w_c = 1$ for $c = \{0, \dots, C - 1\}$, with the background weight $w_C = 0.3$. The loss weights w_{cls} , w_{reg} and w_{count} are set to 1.0, 5e-3, and 1e-4, respectively. The encoder uses ConvNeXt [23]. For SAM and CLIP, we employ their ViT-H [3] and RN50x16 variants, respectively. The category knowledge description texts are jointly designed by pathology experts and GPT-4.

3.2 Comparison Study

On the PanNuke dataset, we followed the experimental setup of [5] and conducted comprehensive evaluations across three folds. We compared multi-class PQ (mPQ) and binary PQ (bPQ) across 19 tissue types, as shown in Tab.1. Our model achieved an overall bPQ of 69.02% and an mPQ of 50.55%. Additionally, we evaluated PQ across five specific categories as shown in Tab.2, attaining an average PQ score of 43.8%, all of which reached state-of-the-art performance.

On the CoNSEP dataset, we compared five semantic segmentation metrics: Dice, AJI, DQ, SQ, and PQ, along with the F1 scores for four different categories as shown in Tab.3. While our model achieved SOTA classification performance, the point-based detection approach still suffered from significant omissions in the densely packed CoNSEP dataset, leading to some performance gaps in semantic metrics. Nevertheless, our method achieved an improvement of 1.6% in AJI and PQ compared to the baseline.

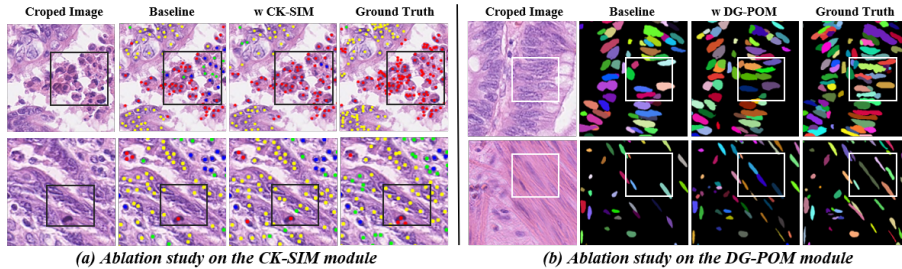


Fig. 3. The visual comparison of ablation study for CK-SIM(a) and DG-POM(b).

Table 4. Ablation study on CoNSEP dataset. The classification and detection results specifically evaluate point prompts.

DG-POM	CK-SIM	Classification			Detection			Segmentation		
		P	R	F	P	R	F	Dice	AJI	PQ
✓	✓	74.68	61.54	66.29	84.08	74.08	78.76	81.06	54.20	53.38
		74.95	63.19	67.55	82.05	77.42	79.66	<u>82.14</u>	<u>55.43</u>	54.07
✓	✓	78.48	62.83	69.33	87.50	74.07	80.22	80.75	54.29	<u>54.61</u>
		<u>75.56</u>	<u>63.01</u>	<u>67.70</u>	85.07	<u>76.88</u>	80.77	82.38	55.83	54.90

3.3 Ablation Study

As shown in Tab.4, we comprehensively evaluate the precision (P), recall (R), and F1-score of point detection and classification obtained by APSeg. Due to space limitations, we only present the ablation experiments on CoNSEP. Additionally, we present the instance segmentation results under the same segmenter using Dice, AJI, and PQ metrics. It can be observed that CK-SIM significantly improves point classification, achieving a 3.04% increase in classification F1-score. Meanwhile, DG-POM enhances instance recall by 3.34%, which greatly benefits segmentation performance, leading to a 1.23% improvement in AJI and a 0.69% increase in PQ. Fig.3 further illustrates the improvements in classification and detection achieved by these two modules. When both modules are used together, the points integrate the advantages of detection and classification, achieving the best segmentation performance.

4 Conclusion

In this paper, we proposed APSeg, an automatic prompt generator for nuclear instance segmentation. APSeg leverages self-acquired knowledge and external knowledge injection to generate more robust prompts. We design and implement a density map-guided proposal offset module and a category knowledge semantic injection module. Extensive comparisons based on the prompt-segment pipeline on the PanNuke and CoNSEP datasets demonstrate the effectiveness and robustness of the prompts generated by APSeg.

References

1. Abdel-Nabi, H., Ali, M., Awajan, A., Daoud, M., Alazrai, R., Suganthan, P.N., Ali, T.: A comprehensive review of the deep learning-based tumor analysis approaches in histopathological images: segmentation, classification and multi-learning tasks. *Cluster Computing* **26**(5), 3145–3185 (2023)
2. Cheng, Z., Wei, Q., Zhu, H., Wang, Y., Qu, L., Shao, W., Zhou, Y.: Unleashing the potential of sam for medical adaptation via hierarchical decoding. In: *Proceedings of the IEEE/CVF Conference on Computer Vision and Pattern Recognition*. pp. 3511–3522 (2024)
3. Dosovitskiy, A., Beyer, L., Kolesnikov, A., Weissenborn, D., Zhai, X., Unterthiner, T., Dehghani, M., Minderer, M., Heigold, G., Gelly, S., et al.: An image is worth 16x16 words: Transformers for image recognition at scale. *arXiv preprint arXiv:2010.11929* (2020)
4. Gamper, J., Alemi Koohbanani, N., Benet, K., Khuram, A., Rajpoot, N.: Pannuke: an open pan-cancer histology dataset for nuclei instance segmentation and classification. In: *Digital Pathology: 15th European Congress, ECDP 2019, Warwick, UK, April 10–13, 2019, Proceedings 15*. pp. 11–19. Springer (2019)
5. Gamper, J., Koohbanani, N.A., Benes, K., Graham, S., Jahanifar, M., Khuram, S.A., Azam, A., Hewitt, K., Rajpoot, N.: Pannuke dataset extension, insights and baselines. *arXiv preprint arXiv:2003.10778* (2020)
6. Graham, S., Vu, Q.D., Raza, S.E.A., Azam, A., Tsang, Y.W., Kwak, J.T., Rajpoot, N.: Hover-net: Simultaneous segmentation and classification of nuclei in multi-tissue histology images. *Medical image analysis* **58**, 101563 (2019)
7. Greenwald, N.F., Miller, G., Moen, E., Kong, A., Kagel, A., Dougherty, T., Fullaway, C.C., McIntosh, B.J., Leow, K.X., Schwartz, M.S., et al.: Whole-cell segmentation of tissue images with human-level performance using large-scale data annotation and deep learning. *Nature biotechnology* **40**(4), 555–565 (2022)
8. Gu, Y., Wu, Q., Tang, H., Mai, X., Shu, H., Li, B., Chen, Y.: Lesam: Adapt segment anything model for medical lesion segmentation. *IEEE Journal of Biomedical and Health Informatics* (2024)
9. He, H., Huang, Z., Ding, Y., Song, G., Wang, L., Ren, Q., Wei, P., Gao, Z., Chen, J.: Cdnnet: Centripetal direction network for nuclear instance segmentation. In: *Proceedings of the IEEE/CVF International Conference on Computer Vision*. pp. 4026–4035 (2021)
10. He, H., Wang, J., Wei, P., Xu, F., Ji, X., Liu, C., Chen, J.: Toposeg: Topology-aware nuclear instance segmentation. In: *Proceedings of the IEEE/CVF International Conference on Computer Vision*. pp. 21307–21316 (2023)
11. Hörst, F., Rempe, M., Heine, L., Seibold, C., Keyl, J., Baldini, G., Ugurel, S., Siveke, J., Grünwald, B., Egger, J., et al.: Cellvit: Vision transformers for precise cell segmentation and classification. *Medical Image Analysis* **94**, 103143 (2024)
12. Kang, S., Moon, W., Kim, E., Heo, J.P.: Vlcounter: Text-aware visual representation for zero-shot object counting. In: *Proceedings of the AAAI Conference on Artificial Intelligence*. vol. 38, pp. 2714–2722 (2024)
13. Kirillov, A., Mintun, E., Ravi, N., Mao, H., Rolland, C., Gustafson, L., Xiao, T., Whitehead, S., Berg, A.C., Lo, W.Y., et al.: Segment anything. In: *Proceedings of the IEEE/CVF International Conference on Computer Vision*. pp. 4015–4026 (2023)
14. Li, H., Zhang, D., Yao, J., Han, L., Li, Z., Han, J.: Asps: Augmented segment anything model for polyp segmentation. In: *International Conference on Medical Image Computing and Computer-Assisted Intervention*. pp. 118–128. Springer (2024)

15. Li, W., Xiong, X., Xia, P., Ju, L., Ge, Z.: Tp-drseg: improving diabetic retinopathy lesion segmentation with explicit text-prompts assisted sam. In: International Conference on Medical Image Computing and Computer-Assisted Intervention. pp. 743–753. Springer (2024)
16. Na, S., Guo, Y., Jiang, F., Ma, H., Huang, J.: Segment any cell: A sam-based auto-prompting fine-tuning framework for nuclei segmentation. arXiv preprint arXiv:2401.13220 (2024)
17. Qin, C., Cao, J., Fu, H., Khan, F.S., Anwer, R.M.: Db-sam: Delving into high quality universal medical image segmentation. In: International Conference on Medical Image Computing and Computer-Assisted Intervention. pp. 498–508. Springer (2024)
18. Radford, A., Kim, J.W., Hallacy, C., Ramesh, A., Goh, G., Agarwal, S., Sastry, G., Askell, A., Mishkin, P., Clark, J., et al.: Learning transferable visual models from natural language supervision. In: International conference on machine learning. pp. 8748–8763. PmLR (2021)
19. Ronneberger, O., Fischer, P., Brox, T.: U-net: Convolutional networks for biomedical image segmentation. In: Medical image computing and computer-assisted intervention—MICCAI 2015: 18th international conference, Munich, Germany, October 5–9, 2015, proceedings, part III 18. pp. 234–241. Springer (2015)
20. Shi, H., Han, S., Huang, S., Liao, Y., Li, G., Kong, X., Zhu, H., Wang, X., Liu, S.: Mask-enhanced segment anything model for tumor lesion semantic segmentation. In: International Conference on Medical Image Computing and Computer-Assisted Intervention. pp. 403–413. Springer (2024)
21. Shui, Z., Zhang, Y., Yao, K., Zhu, C., Zheng, S., Li, J., Li, H., Sun, Y., Guo, R., Yang, L.: Unleashing the power of prompt-driven nucleus instance segmentation. In: European Conference on Computer Vision. pp. 288–304. Springer (2025)
22. Sun, G., An, Z., Liu, Y., Liu, C., Sakaridis, C., Fan, D.P., Van Gool, L.: Indiscernible object counting in underwater scenes. In: Proceedings of the IEEE/CVF Conference on Computer Vision and Pattern Recognition. pp. 13791–13801 (2023)
23. Woo, S., Debnath, S., Hu, R., Chen, X., Liu, Z., Kweon, I.S., Xie, S.: Convnext v2: Co-designing and scaling convnets with masked autoencoders. In: Proceedings of the IEEE/CVF conference on computer vision and pattern recognition. pp. 16133–16142 (2023)
24. Wu, J., Ji, W., Liu, Y., Fu, H., Xu, M., Xu, Y., Jin, Y.: Medical sam adapter: Adapting segment anything model for medical image segmentation. arXiv preprint arXiv:2304.12620 (2023)
25. Xiong, X., Wu, Z., Tan, S., Li, W., Tang, F., Chen, Y., Li, S., Ma, J., Li, G.: Sam2-unet: Segment anything 2 makes strong encoder for natural and medical image segmentation. arXiv preprint arXiv:2408.08870 (2024)
26. Yao, K., Huang, K., Sun, J., Hussain, A.: Pointnu-net: Keypoint-assisted convolutional neural network for simultaneous multi-tissue histology nuclei segmentation and classification. *IEEE Transactions on Emerging Topics in Computational Intelligence* **8**(1), 802–813 (2023)
27. Yue, W., Zhang, J., Hu, K., Xia, Y., Luo, J., Wang, Z.: Surgicalsam: Efficient class promptable surgical instrument segmentation. In: Proceedings of the AAAI Conference on Artificial Intelligence. vol. 38, pp. 6890–6898 (2024)
28. Zhang, Y., Zhou, T., Wang, S., Liang, P., Zhang, Y., Chen, D.Z.: Input augmentation with sam: Boosting medical image segmentation with segmentation foundation model. In: International Conference on Medical Image Computing and Computer-Assisted Intervention. pp. 129–139. Springer (2023)